

Three-dimensional Hysteresis Compensation Enhances Accuracy of Robotic Artificial Muscles

Jun Zhang, Anthony Simeonov and Michael C. Yip

Abstract—Robotic artificial muscles are compliant and can generate straight contractions. They are increasingly popular as driving mechanisms for robotic systems. However, their strain and tension force often vary simultaneously under varying loads and inputs, resulting in three-dimensional hysteretic relationships. The three-dimensional hysteresis in robotic artificial muscles poses difficulties in estimating how they work and how to make them perform designed motions. This study proposes an approach to driving robotic artificial muscles to generate designed motions and forces by modeling and compensating for their three-dimensional hysteresis. The proposed scheme captures the nonlinearity by embedding two hysteresis models. The effectiveness of the model is confirmed by testing three popular robotic artificial muscles. Inverting the proposed model allows us to compensate for the hysteresis among temperature surrogate, contraction length, and tension force of a shape memory alloy (SMA) actuator. Feedforward control of an SMA-actuated robotic bicep is demonstrated. This study can be generalized to other robotic artificial muscles, thus enabling muscle-powered machines to generate desired motions.

Index Terms—Robotic artificial muscles, hysteresis, inverse compensation, shape memory alloy actuator.

I. INTRODUCTION

ARTIFICIAL muscles are broadly defined as materials that can change their shapes under external chemical or physical stimuli [1], [2]. In this study, we define a subset of artificial muscles as robotic artificial muscles, which can generate straight contractions in their cross-sectional directions during activation. Although conventional technologies such as electric motors and hydraulic actuators can be well characterized to operate effectively, they are non-ideal in many situations where their form factor, force, size, and weight do not properly match an application’s needs. Robotic artificial muscles, such as shape memory alloy (SMA) actuators, McKibben actuators, and super-coiled polymer (SCP) actuators (Fig. 1(a)-(c)), offer many advantages over conventional technologies in terms of power-to-weight ratio, force-to-weight ratio, and inherent compliance [3]. They can be utilized as driving mechanisms for robotic systems and have shown strong potential in novel robotic applications such as safe human-robot interaction, legged robotics, robotic prostheses and orthoses, and soft robotics.

To practically employ robotic artificial muscles, it is crucial to understand how they work and how to make them generate designed motions and forces. The full utilizations of robotic artificial muscles are challenged by the three-dimensional and

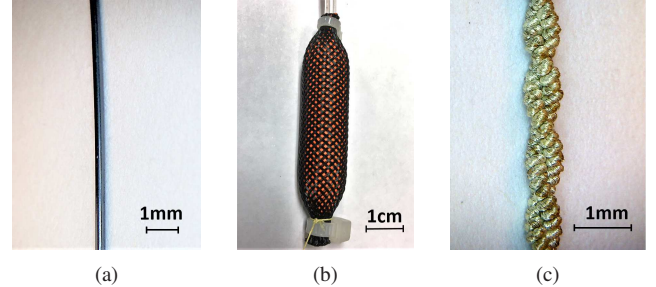


Fig. 1. Popular robotic artificial muscles. (a). A Flexinol shape memory alloy (SMA) actuator (Dynalloy, Inc). (b). A McKibben actuator. (c). A super-coiled polymer (SCP) actuator.

coupled hysteresis – any of the two variables among input, strain, and tension force are often hysteretic (Fig. 2). In practical applications, such as an SMA-actuated robot hand for grasping an object with different temperatures and weights, the strain and tension force of the SMA actuators would vary under varying loads and inputs, resulting in complicated hysteretic relationships. There have been limited studies on three-dimensional hysteresis models with coupled variables for robotic artificial muscles. Furthermore, the hysteresis properties of different artificial muscles are often different, thus a generalizable and data-driven modeling and control methodology is highly desirable.

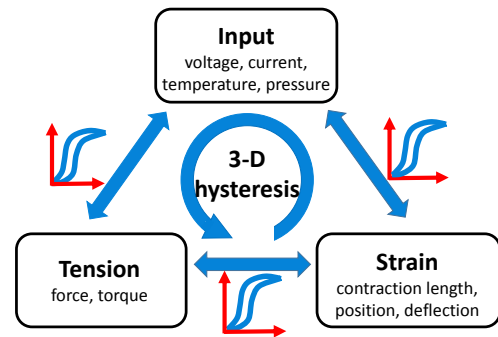


Fig. 2. Three-dimensional hysteresis in robotic artificial muscles.

This study proposes an approach to describing, estimating, and compensating for the three-dimensional hysteresis in robotic artificial muscles. The proposed method is used to drive robotic artificial muscles to generate designed motions and forces. The effectiveness of the proposed model is confirmed by testing the modeling performance for the hysteresis behaviors in an SMA actuator, a McKibben actuator, and an SCP actuator. The proposed method enables accurate compensation for the hysteresis in a broad range of robotic

Jun Zhang and Michael C. Yip are with the Department of Electrical and Computer Engineering, University of California, San Diego, La Jolla, CA 92093, USA (email: j5zhang@ucsd.edu; yip@ucsd.edu).

Anthony Simeonov is with the Department of Mechanical and Aerospace Engineering, University of California, San Diego, La Jolla, CA 92093, USA (email: asimeono@ucsd.edu).

artificial muscles and further facilitates roboticists to drive machines powered by robotic artificial muscles to generate designed motions. This work extends our recent conference paper [4] in the following aspects: (1) the verification of the proposed model for a McKibben actuator and an SCP actuator, (2) the derivation and experimental validation of the inverse compensation algorithm for the three-dimensional hysteresis in an SMA actuator, (3) the feedforward angle control of an SMA-actuated robotic bicep system, and (4) the improved structure and presentation throughout the paper.

The main contributions of this paper are as follows:

- 1) An accurate and generalizable model for characterizing and estimating the three-dimensional hysteresis in different robotic artificial muscles. The proposed scheme captures the nonlinearity by recursively embedding two hysteresis models. The adopted embedding procedure results in a more superior modeling capability than other approaches, as briefly discussed in Section III.B and detailed in [4].
- 2) The derivation of the inverse algorithm to compensate for the three-dimensional hysteresis based on the proposed model. We show that inverting the proposed model allows us to compensate for the hysteresis among input, contraction length, and tension force of an SMA actuator for position and force control. To show its use in practice, the feedforward angle control of an SMA-actuated robotic bicep is demonstrated, where strain and tension force are coupled and vary continuously.

II. RELATED WORK

Several popular robotic artificial muscles exhibiting three-dimensional hysteresis are highlighted:

SMA Actuators: SMAs are a class of materials that can contract and elongate under stimulus such as thermomechanical variation [5]. They have been widely utilized in robotic systems [6]–[8]. However, the characterization of the hysteresis among temperature, strain, and tension force was a challenging task [5], [8]. A number of physics-based models have been proposed, but the analysis was often constrained to particular types of SMAs and could not faithfully capture the hysteresis [9]. The full derivation of these models was often complicated since molecular-level physics was used [10]. Phenomenological models that did not depend on physics have also been proposed; however, the existing methods could only capture the hysteresis between two domains and were thus limited in many applications where strain and tension force varied simultaneously. For example, a Preisach model was employed for current – strain hysteresis of an SMA actuator [11], but under a constant tension force. An adaptive neuro-fuzzy inference system model was realized for an SMA actuator at various frequencies, but only the voltage – strain hysteresis was captured [12]. Similarly, a generalized Prandtl-Ishlinskii model was adopted for position control, only the temperature – deflection hysteresis was compensated [13]. The existing methods could not faithfully capture or compensate for the three-dimensional and coupled hysteresis in SMA actuators.

McKibben Actuators: Pneumatic artificial muscles, such as the McKibben actuators, can convert energy from compressed air to mechanical motion. They can be directly coupled to a mechanical joint without additional gearing mechanisms [14]. While they have been utilized in various robotic applications [15], [16], the hysteresis brought difficulties in modeling and controlling these artificial muscles [14]. Although static models have been derived, the hysteresis was often not captured [16], [17]. The pressure – length hysteresis of a dual pneumatic artificial muscle system was modeled by a series of Prandtl-Ishlinskii models [18], the experiment focused on isobaric cases, and the overall model was complex since an individual model was employed for the system under a particular pressure. In [19], a Maxwell-slip model was proposed as a lumped-parametric model for pneumatic artificial muscles. The virgin curve equation was adopted to describe the friction force. Since it only considered isotropic friction, the proposed model could not capture the hysteresis among pressure, strain, and tension force simultaneously.

SCP Actuators: SCP actuators can generate large contractions when thermally activated. They have demonstrated significant mechanical power and good dynamic range [20], [21], thus is a compelling robotic artificial muscle [22]. SCP actuators could be manufactured by continuously twisting carbon nanotube yarns, nylon fishing lines, or sewing threads until coils were formed [21]. It was known that hysteresis resulted from the friction of the coiled threads [21], [22], and could cause up to 30% strain difference under the same input [23]; however, the majority of the existing studies either utilized linear models [22], [24], [25] or complicated physical models [26], both of which failed to capture the hysteresis among temperature, strain, and tension force. A hysteresis model was adopted for an SMA-fishing-line actuator, but the analysis assumed constant tension force [27]. We recently proposed an approach to capture and compensate for the voltage – strain hysteresis in an SCP actuator, but the strain – tension force hysteresis was approximated as a polynomial term [23].

Modeling and control of systems with two-dimensional hysteresis has been an active research area. Unlike physics-based models which were derived based on material properties [10], [28], phenomenological models (i.e. Preisach model, Krasnoselskii-Pokrovskii model, Prandtl-Ishlinskii model, Maxwell-Slip model, Duhem model, and Bouc-Wen model) were directly derived based on numerical data and could often capture different hysteresis behaviors [19], [29]–[33], thus were more widely utilized. With success in modeling, a significant amount of effort has been spent on the control of hysteretic systems. A predominant class of feedforward control strategies involved approximate cancellation of the hysteresis through inverse compensation [34]–[38]. For example, in [36], an analytical inverse of a generalized Prandtl-Ishlinskii model was derived and experimentally validated. A nonlinear inverse filter was constructed to compensate for the hysteresis in a galfenol actuator [34]. Furthermore, to improve the control performance, feedback controls have been developed. Traditional methods like the proportional-integral-derivative controls and more advanced methods [13], [38] have

been implemented in a variety of systems.

The Preisach model was one of the most effective two-dimensional hysteresis models that has been widely adopted [31], [32], [35]. The model was formulated by a weighted superposition of delayed relays. Practical model implementation involved discretization of the model parameters (weight function) to obtain a finite number of parameters [32]. The identification of the Preisach model could often be solved efficiently [31], [35]. In this study, we adopted the Preisach model and its inverse to construct the proposed modeling and compensation approach, because the Preisach model had a proven modeling capability for saturated and asymmetric hysteresis behaviors [31], [35], [39], [40] and its inverse could be numerically computed [31]. However, new methods are required since the hysteresis in robotic artificial muscles is three-dimensional and coupled.

Compared to two-dimensional hysteresis, multi-dimensional hysteresis is significantly more challenging to deal with – the task of collecting sufficient data to cover the parameter space becomes significantly more burdensome. Very few strategies on multi-dimensional scenarios exist, and they have some noticeable limitations for the hysteresis in robotic artificial muscles. A vector Preisach model was proposed to capture the isotropic hysteresis of the magnetization process [41]; however, the amplitude and phase inputs were considered to be independent but not coupled. A multi-dimensional Bouc-Wen model was presented to compensate for the hysteresis in a two-degree-of-freedom piezoelectric actuator [29]; however, the modeling capability was limited due to a low number of parameters. A multi-dimensional Prandtl-Ishlinskii model was presented [42], but each input was assumed to independently influence the output. The inverse of a multi-dimensional Prandtl-Ishlinskii model was further derived [43], but the model was additively formulated, which did not necessarily work for robotic artificial muscles. A recently proposed coupled Prandtl-Ishlinskii model was also based on an additive formulation [44]. We proposed a composite model for the hysteresis among current, resistance, and deflection of a vanadium dioxide microactuator [38], but the model was intrinsically two-dimensional since the resistance was an intermediate variable solely dependent on the current. Thus, despite several studies catering to specific applications, the general problem of three-dimensional and coupled hysteresis in robotic artificial muscles remains unsolved.

III. CHARACTERIZATION AND DISCUSSION

A. Characterization

In this study, we chose the SMA actuators as the main example to test the proposed method, considering that they could be electrically controlled and have been widely used in robotic applications. SMA actuators exhibit three-dimensional hysteresis among temperature, strain, and tension force. Note that other robotic artificial muscles might have alternative hysteretic elements (e.g., pressure for McKibben actuators). The strain was quantified as the contraction length, and was defined as the change of actuator length with respect to its resting length. The contraction length increased when the

actuator was elongated, and decreased during contraction. Due to the lack of sensitive temperature sensors for thin muscle-form factors, it was difficult to directly and accurately measure the temperature of SMA actuators. Thus, the voltage applied across the SMA actuator, resulting in Joule heating, was used as a temperature surrogate $q(T) = V$.

To fully capture the hysteresis, a series of static relationships were obtained based on a temperature surrogate ($q(T)$), contraction length (L), and tension force (F) measurement system. Since the time constant of the thermal dynamics was approximately 5 s, each voltage step was held for 30 s to ensure that the steady-state values were reached. Note that this experiment was to obtain the static hysteresis, by incorporating the thermal dynamics of the system ([9], [22], [45]), accurate model predictions could be achieved for faster motions.

We began by capturing the two-dimensional hysteresis between F and $q(T)$, L and $q(T)$, and L and F :

F – q(T) Hysteresis: The hysteresis between tension force and temperature surrogate was obtained when the actuator was close to its resting length. A small pre-tension of 0.5 N was utilized to prevent the actuator from being slack under low voltages. Fig. 3(a) shows the corresponding hysteresis measurements. The force range was [0.5, 15.2] N, and the voltage range was [0, 6] V.

L – q(T) Hysteresis: The hysteresis between contraction length and temperature surrogate under different tension forces was captured. Tension forces were generated by attaching weights to the actuator. A position sensor was utilized to measure the contraction length. Since the actuator length changed with different loading forces, the initial contraction length values of each hysteresis curve were different, implying that a single two-dimensional hysteresis model is not sufficient. The hysteresis curves were saturated at low and high temperatures and are asymmetric (Fig. 3(b)).

L – F Hysteresis: The hysteresis between contraction length and tension force was obtained under constant temperatures (Fig. 3(c)). The initial forces were close to zero, and the initial contraction lengths of different hysteresis curves were different. The hysteresis curves under different temperatures exhibited different profiles, further complicating the modeling.

In practical applications, it is often desirable to control the strain and the tension force of SMA actuators to follow designed sequences by applying voltages – the modeling and compensation of the $F – q(T)$ hysteresis and the $L – q(T)$ hysteresis are thus treated in detail in this study.

B. What should be a Good Model for Robotic Artificial Muscles?

From Fig. 3, it is seen that the relationship between contraction length, force, and temperature surrogate of the SMA actuator is hysteretic and coupled together. The hysteresis curves exhibit different shapes under different conditions. Individual hysteresis model could be separately identified and then combined to obtain the overall model. However, then the model will be overly complicated. This work attempts to propose an efficient three-dimensional model that can capture the coupled hysteresis.

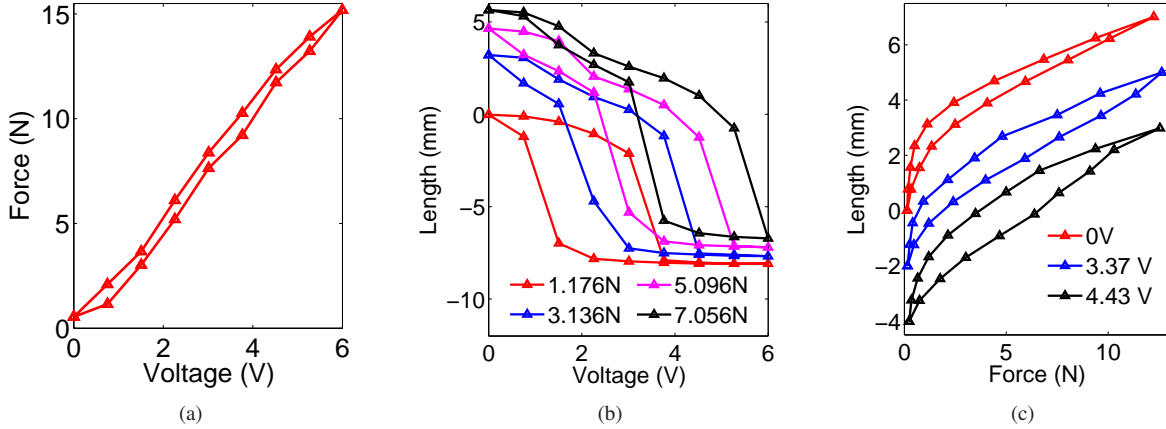


Fig. 3. The three-dimensional hysteresis of an SMA actuator between the (a) $F-q(T)$, (b) $L-q(T)$, and (c) $L-F$ hysteresis.

Denote H_i , $i = 1, 2, \dots, 5$ are Preisach models with different parameters. Without loss of generality, L is the output, F and $q(T)$ are inputs. One option is that the length is expressed as the weighted summation of two independent hysteresis models: $L = H_3[F] - H_4[q(T)]$. A similar additive multivariable hysteresis model has been proposed [43]. However, this approach only works for cases where all of the hysteresis curves have similar profiles except with different offsets. For example, the hysteresis between L and $q(T)$ would be the same except with a shift under a different constant F , which is not true for SMA actuators, as shown in Fig. 3(b). Another option is to simplify the relationship between F and $q(T)$ as linear, and embed the linear relationship into the overall model as $L = H_5[F - a_1 \cdot q(T) - a_0]$, where a_0 and a_1 are constants. Although this model can generate different $L-q(T)$ hysteresis curves under different constant F , the $F-q(T)$ relationship is simplified to be hysteresis-free and linear, which would generate significant errors if the $F-q(T)$ relationship is hysteretic. The above two approaches have been tested to be ineffective for SMA actuators in our recent study [4].

In this study, we propose a model that can effectively capture and estimate the full hysteresis relationships by embedding a two-stage Preisach model: the proposed approach first characterizes the $F-q(T)$ hysteresis as $F = H_1[q(T)]$ when the actuator is close to its resting length, and then embeds the relationship into the overall model as $L = H_2[F - H_1[q(T)]]$. Compared to the aforementioned approaches, the proposed method is more accurate [4]. The detailed derivation of the model is provided in Section IV.

IV. THREE-DIMENSIONAL HYSTERESIS MODELING

To model the hysteresis shown in Fig. 3, a group of two-dimensional hysteresis models could indeed be employed, but the computation would be overly complicated. In this section, an efficient three-dimensional hysteresis model is proposed for capturing the hysteresis in robotic artificial muscles. The formulation and identification of the model are described. Though we describe the following sections with Temperature as the input and Tension and Strain as the inter-coupled hysteretic

outputs, it is important to point out that the formulations are generalizable for different forms of input (i.e. temperature, current, pressure, etc.) and are therefore valid for robotic artificial muscles with different activation mechanisms.

A. Steady-state Voltage as Temperature Surrogate

The independent variables describing the SMA actuators are temperature, contraction length, and tension force. Direct temperature measurement of the SMA actuator is a challenging task – the SMA actuators utilized in this work had a diameter of 0.203 mm, and conventional thermocouples or laser thermometers could not work properly at such a small scale. To obtain the temperature of the SMA actuator, we adopted the concept of temperature surrogate [38]. Based on existing thermal models of the SMAs, the constant (quasi-static) voltage V could be expressed as a single-valued and monotonically increasing function of T , namely, $V = q(T)$.

For illustration purposes, we provided an example based on the thermal model of Joule heating [45]. The thermo-electric model of the SMA actuators was written as

$$\frac{dT(t)}{dt} = -d_1(T(t) - T_0) + d_2V^2(t), \quad (1)$$

where d_1 and d_2 were positive constants relevant to the density, volume, heat transfer coefficient, resistance, and surface area of the SMA actuators, and T_0 was the ambient temperature. This model has been validated in [22], [38]. It is noted that the resistance of the SMA actuators might undergo mild changes during phase transition – the resistance change was less than 15% [46] and was approximated to be constant.

Under a constant voltage V , the steady-state temperature T would be reached. V could be expressed in terms of T :

$$V = \sqrt{\frac{d_1}{d_2}(T - T_0)} = q(T). \quad (2)$$

The function $q(T)$ in Eq. (2) was indeed single-valued and strictly increasing, and thus was a legitimate surrogate for T .

Under dynamic conditions, the temperature of the SMA actuators cannot be directly correlated with voltage based on

Eq. (2); however, the relationship between temperature and voltage is available, as expressed in Eq. (1). By identifying the additional model parameters in Eq. (1) and combining it with the proposed model, the performance of SMA actuators can still be modeled. This study proposes modeling and compensation methods considering the surrogate temperature based on Eq. (2), and the consideration of the temperature in dynamic conditions is a future study of this work.

B. Proposed Model

The proposed model was constructed from embedding two Preisach models.

1) $F - q(T)$ Hysteresis: A Preisach model with parameter (weight function) ω was adopted to model the $F - q(T)$ hysteresis under resting length condition ($L \approx 0$):

$$\begin{aligned} F(t) &= H_1[q(T(\cdot)); \zeta_0](t) \\ &= \int_{\mathcal{P}_0} \omega(\beta, \alpha) \gamma_{\beta, \alpha}[q(T(\cdot)); \zeta_0(\beta, \alpha)](t) d\beta d\alpha + c_0, \end{aligned} \quad (3)$$

where \mathcal{P}_0 was the Preisach plane and defined as

$$\mathcal{P}_0 \triangleq \{(\beta, \alpha) : q(T_{\min}) \leq \beta \leq \alpha \leq q(T_{\max})\}, \quad (4)$$

$[q(T_{\min}), q(T_{\max})]$ was the temperature surrogate (quasi-static voltage) range, $\gamma_{\beta, \alpha}$ was the hysteron, which was the basic element of the Preisach model, c_0 was a constant bias.

The output of the hysteron at time t depended on the current and the history of the temperature surrogate $q(T(\tau))$, $0 \leq \tau \leq t$. $\zeta_0(\beta, \alpha) \in \{-1, 1\}$ was the initial hysteron output, the hysteron at t could be expressed as:

$$\gamma_{\beta, \alpha}[q(T(\cdot)); \zeta_0(\beta, \alpha)](t) = \begin{cases} +1 & \text{if } q(T(t)) > \alpha \\ -1 & \text{if } q(T(t)) < \beta \\ \zeta_0(\beta, \alpha) & \text{if } \beta \leq q(T(t)) \leq \alpha. \end{cases} \quad (5)$$

Practical model implementation involved discretization of the weight function ω to obtain a finite number of parameters. The weight function was approximated as a piecewise constant function – the weight w_{ij} was constant within cell (i, j) , $i = 1, 2, \dots, N_1$; $j = 1, 2, \dots, N_1 - i + 1$, where N_1 was the discretization level and $\{w_{ij}\}$ were the model parameters. The discretization level is often empirically determined by considering the accuracy and complexity of the discretized model [31]. The weights were usually constrained to be either non-negative or non-positive such that the resulted model could describe monotonic hysteresis [31], [35].

At time n , the output of the discretized Preisach model could be expressed as

$$F(n) = H_1[q(T(n))] = \sum_{i=1}^{N_1} \sum_{j=1}^{N_1+1-i} w_{ij} s_{ij}(n) + c_0, \quad (6)$$

where w_{ij} was the weight for cell (i, j) , and $s_{ij}(n)$ was the signed area of the cell (i, j) , which was fully determined by the temperature surrogate $q(T)$ up to time n .

Note that $L \approx 0$ and L was assumed not present in the model. Since a small pre-tension of 0.5 N was used, $H_1(0) = 0.5$ N.

The model parameters consisted of the weights $\{w_{ij}\}$ and the constant bias c_0 .

2) $L - F - q(T)$ Hysteresis: $F(n) = H_1[q(T(n))]$ (Eq. (6)) held only when $L(n)$ was zero. By embedding the $F - q(T)$ hysteresis, a three-dimensional model among L , F , and $q(T)$ was formulated as

$$L(n) = H_2[F(n) - H_1[q(T(n))]] = \sum_{i=1}^{N_2} \sum_{j=1}^{N_2+1-i} \mu_{ij} p_{ij}(n) + c_1, \quad (7)$$

where N_2 was the discretization level for H_2 , $\{\mu_{ij}\}$ were the parameters of the model, and c_1 was a constant bias. Considering that the hysteresis between F and $q(T)$ was embedded, $F - H_1[q(T)]$ was the input of the high-level hysteresis model H_2 . The negative term of $H_1[q(T)]$ was introduced due to the fact that the hysteresis between contraction length and temperature surrogate was monotonically decreasing (Fig. 3(b)).

When the tension force was close to zero and no voltage was applied, the actuator would remain its resting length, so $H_2(0) = 0$ mm.

3) Model Identification: The identification of the $F - q(T)$ hysteresis model, H_1 in Eq. (6), could be reformulated as a constrained linear least-squares problem and solved efficiently with the MATLAB command `lsqnonneg` [31], [35], [38].

After the identification of H_1 , the identification of the proposed model, H_2 in Eq. (7), could also be efficiently realized by the linear least-squares algorithm. For ease of presentation, the model parameters were rewritten in the following vector form:

$$D = (d_1 \quad d_2 \quad \dots \quad d_{N_2(N_2+1)/2} \quad c_1)^\top, \quad (8)$$

where $d_k = \mu_{ij}$, $k = (i-1)(2N_2-i+2)/2 + j - 1$. The input sequence was denoted as $F(n) - H_1[q(T(n))]$, $n = 1, 2, \dots, N$, and the corresponding $p_{ij}(n)$ could be calculated by tracking the evolution of the input history up to time n . By stacking $p_{ij}(n)$ into a row of a matrix: $P(n, k) = p_{ij}(n)$, and $P(n, N_2(N_2+1)/2 + 1) = 1$. The output of the model $\tilde{L} = (\tilde{L}(1) \quad \tilde{L}(2) \quad \dots \quad \tilde{L}(N))^\top$ could be expressed as

$$\tilde{L} = PD. \quad (9)$$

Denote the experimental contraction length measurement under input sequence $z(n) = F(n) - H_1[q(T(n))]$, $n = 1, 2, \dots, N$, as

$$Z = (z(1) \quad z(2) \quad \dots \quad z(N))^\top. \quad (10)$$

The model parameters, D , could be calculated such that $\|PD - Z\|_2^2$ was minimized under the sign constraints of the weights. The weights of $\{\mu_{ij}\}$ were constrained to be non-negative in this study.

If the hysteresis is relatively small, the resulted weights of the Preisach model will be primarily located close to the $\beta = \alpha$ line. If the hysteresis is more significant, a larger portion of the major weights will be located away from the $\beta = \alpha$ line. More details about the Preisach model can be found in [23], [31], [32], [35], [38], [41].

C. Linear Model

Since the linear model had a low computational cost and an efficient inverse model, this approach has been widely adopted in existing studies [14], [16], [22], [35], where the hysteresis behavior was roughly approximated as a linear or polynomial relationship. By simplifying the relationship between F and $q(T)$ as linear, and embedding the relationship into an overall linear expression, the linear model was adopted as a comparison method:

$$L = k_2(F - k_1 \cdot q(T) - F_0), \quad (11)$$

where k_1 , k_2 and F_0 were constants. F_0 was the pre-tension term. The model identification was realized with the linear regression algorithm using MATLAB command *polyfit*. This is a “no hysteresis” model – it simplified the hysteretic relationships to be hysteresis-free and linear, thus would generate significant errors. Furthermore, this approach could not capture the shape differences among different hysteresis curves. For example, when the tension force changed from a constant value, F , to another constant value, F' , the only effect to the modeled $L - q(T)$ profile was a changed offset $k_2 \cdot (F' - F)$.

V. THREE-DIMENSIONAL HYSTERESIS COMPENSATION

In this section, we describe how to invert the three-dimensional hysteresis model, and how to realize feedforward control of an SMA actuator and an SMA-actuated robotic bicep system.

A. Inverse Compensation Algorithm

1) *Proposed Algorithm*: Inverse compensation is a feedforward control scheme widely adopted for nonlinear systems [31]. An inverse hysteresis strategy can be employed to approximately cancel out the system hysteresis (Fig. 4(a)).

Considering that the proposed model was constructed based on a two-stage Preisach model, a corresponding two-stage inverse was derived to invert the proposed model. The derived inverse algorithm could be employed for tension force control and contraction length control of SMA actuators, such that tension force and contraction length could follow desired sequences.

Denote the reference tension force as F_d , the goal of inverse compensation was to find the required temperature surrogate (voltage step) input $\widehat{q(T)}$, such that $F_d \approx H_1[\widehat{q(T)}]$. The input $\widehat{q(T)}$ could be calculated by inverting H_1 as

$$\widehat{q(T(n))} \approx H_1^{-1}[F_d(n)]. \quad (12)$$

While the inverse of the Preisach model was not provided here, the detailed analysis could be found in [31], [35], [37].

Further denote the reference contraction length as L_d , the goal was to find $\widehat{q(T)}$, such that $L_d \approx H_2[F_d - H_1[\widehat{q(T)}]]$. This could be realized by inverting H_2 and H_1 sequentially. First, the input of the high-level model H_2 , $F_d - H_1[\widehat{q(T)}]$, was obtained by inverting H_2 :

$$F_d(n) - H_1[\widehat{q(T(n))}] \approx H_2^{-1}[L_d(n)]. \quad (13)$$

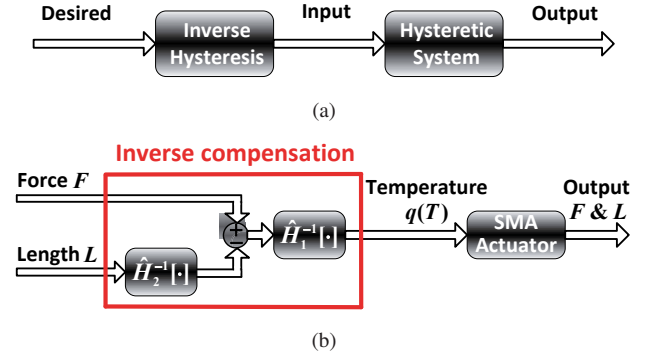


Fig. 4. Illustration of the inverse compensation of (a) a general hysteretic system, and (b) the three-dimensional hysteresis in SMA actuators.

The input $\widehat{q(T)}$ could then be calculated by inverting H_1 as

$$\widehat{q(T(n))} \approx H_1^{-1}[F_d(n) - H_2^{-1}[L_d(n)]]. \quad (14)$$

Eq. (14) was the inverse of the proposed model, and the scheme was also illustrated in Fig. 4(b).

It is noted that other possible model inverse expression can be derived, depending on the model expression. For example, when F is chosen to be the output, L and $q(T)$ are inputs, the length - voltage model and force - length model can be adopted for inverse. In practical applications, it is often desirable that the SMA actuator produces a sequence of predefined force or strain values [32], [38]. To solve such a problem, the proposed inverse algorithm is utilized multiple times.

2) *Linear Model Inverse*: The inverse of the linear model could be conveniently realized. Given the reference contraction length and tension force, the input $\widehat{q(T)}_L$ could be obtained as

$$\widehat{q(T)}_L = \frac{1}{k_1}(F_d - F_0 - \frac{L_d}{k_2}). \quad (15)$$

This approach was implemented to control the tension force and contraction length of the SMA actuator as a comparison. Unlike the inverse of the Preisach model, the inverse of the linear model was another linear function.

B. Feedforward Control of Robotic Bicep

Applications such as robotic arms [16], [22], rehabilitation robots [15], medical robots [9], biomimetic robots [7], and soft robots [6], are prime systems for robotic artificial muscles to be implemented. To show the use of the proposed method in practice, a one-link robotic bicep actuated by three SMA actuators (Fig. 5(a)-(b)) was chosen in this study. Admittedly simple, similar working mechanisms have been widely used [16]. Furthermore, the changes in temperature, strain, and tension force of the SMA-actuated robotic bicep were continuous. This was different from the experimental testing of an SMA actuator, where the tension force change was discrete and realized by manually adding weights. The proposed method in this study can be further applied to more sophisticated systems powered by multiple robotic artificial muscles since each of them can be individually modeled and controlled.

In feedforward control of the robotic bicep, the goal was to calculate the control input such that if applied, the system could achieve a desired static configuration. The schematic of the robotic bicep was provided (Fig. 5(c)). The control variable was chosen to be the angle of the robotic bicep, θ , which was defined as the angle between the forearm and the upward vertical direction.

1) *Quasi-static Analysis*: Quasi-static equilibrium analysis of the robotic bicep was conducted (Fig. 5(c)). Given the weight at the end of the bicep, m_{weight} , the weight of the forearm itself, m_{arm} , and the system configuration, the actuator tension force to maintain equilibrium was calculated as the angle varied throughout the operating range. The known quantities of the system configuration were the distance from the pivot (A) to the clamp along the arm, x ; the height of the clamp, a ; the vertical distance from the pivot (A) to the top actuator connection point (D), y ; and the length of the forearm, l . The bicep angle, θ , was defined as the angle between the forearm and the upward vertical direction. The combined tension force of the three SMA actuators, $3F$, was calculated using the following moment balance:

$$3Fr = m_{\text{weight}}gl \sin \theta + \frac{m_{\text{arm}}gl \sin \theta}{2}, \quad (16)$$

where the center of mass of the bicep was assumed to be in the center of the forearm. This was a legitimate assumption since a uniform aluminum rod was used as the forearm. The additional moment introduced by the clamp was not included in the analysis, considering that the clamp was very close to the pivot, and its mass was significantly less than the aluminum rod.

The perpendicular distance from the pivot point to the actuator force line of action ($r = AR$) was calculated in the following derivations: first, line segment $c = AC$ and the angle γ between line segment AC and the forearm, were determined using right triangle relationships as

$$\begin{aligned} c^2 &= a^2 + x^2, \\ \gamma &= \tan^{-1}(a/x). \end{aligned} \quad (17)$$

Then, denote $\kappa = \theta - \gamma$, the contraction length of the actuator was obtained by using the law of cosine relationship as

$$L = z_0 - \sqrt{c^2 + y^2 - 2cy \cos(\kappa)}, \quad (18)$$

where z_0 was the resting length of the actuator. Angle δ between the actuators and the downward vertical direction could be determined as

$$\delta = \frac{\cos^{-1}(c^2 - z^2 - y^2)}{-2zy}, \quad (19)$$

where z was the current length of the actuator and could be obtained from Eq. (18). Finally, r could be calculated from $r = y \sin \delta$. The tension force of each SMA actuator was obtained:

$$F = \frac{1}{3} \cdot \frac{(2m_{\text{weight}} + m_{\text{arm}})gl \sin \theta}{2y \sin \delta}. \quad (20)$$

2) *Feedforward Control*: Under the quasi-static condition, the angle θ of the robotic bicep determined the tension force F and the contraction length L of the SMA actuators. It was calculated that when the system was under an equilibrium angle θ_d , the corresponding contraction length of the actuators L_d was

$$L_d = z_0 - \sqrt{c^2 + y^2 - 2cy \cos(\theta_d - \gamma)}. \quad (21)$$

The corresponding tension force F_d of each SMA actuator was

$$F_d = \frac{(2m_{\text{weight}} + m_{\text{arm}})gl \sin \theta_d}{6y \sin \delta}. \quad (22)$$

With the computed contraction length (Eq. (21)) and tension force (Eq. (22)) of the SMA actuators, the control inputs, $q(T)$, could be calculated based on the proposed compensation scheme (Eq. (14)) or the inverse of the linear model (Eq. (15)).

VI. EXPERIMENTAL SETUP

A. SMA Actuator

The experimental testbed (Fig. 6) consisted of an SMA actuator (Dynalloy, Inc) with a resting length of 27 cm and a diameter of 0.203 mm, a position sensor (SPS-L035-LATS, Honeywell) with 0.04 mm resolution for contraction length measurement, a load cell (LSP-2, Transducer Techniques) to measure the tension force, and a servo motor (MX-28, Dynamixel) with an aluminum capstan to control the length of the SMA actuator. Similar to [4], [22], [23], a tangential blower fan (QG030-198/12, Ebm-papst) was utilized to provide an approximately even airflow environment. The SMA actuator had a dark blue color and was highlighted with a more bright color for visualization purposes. Contraction length measurement was performed by accurately sensing the position of a magnet with an array of magnetoresistive sensors. The magnet and the weights were hung on the actuator to generate tension forces. The weights containing ferrous metals were kept a distance from the magnet to ensure accurate measurements. The additional mass of the magnet and components hung on the actuator was 20 g. Fig. 6(a) shows the setup for $L - q(T)$ hysteresis measurement, and Fig. 6(b) shows the setup for $F - q(T)$ and $L - F$ hysteresis measurements. Temperature surrogate was realized by applying voltage steps with a pulse-width-modulated circuit. Data acquisition was realized in LabVIEW software.

The SMA actuator with a diameter of 0.203 mm was chosen in this work since they produced large forces (15 N) and exhibited fast responses (time constant closes to 5 s). As the SMA actuator became thicker, the response became slower. Note that since the proposed approach was based on a phenomenological model (Preisach model), this study applied to SMA actuators with other diameters and materials, as well as other types of robotic artificial muscles.

B. Robotic Bicep

A one-link robotic bicep system actuated by three SMA actuators in parallel was developed (Fig. 5(a)). The system consisted of a mounted vertical structure made of plywood,

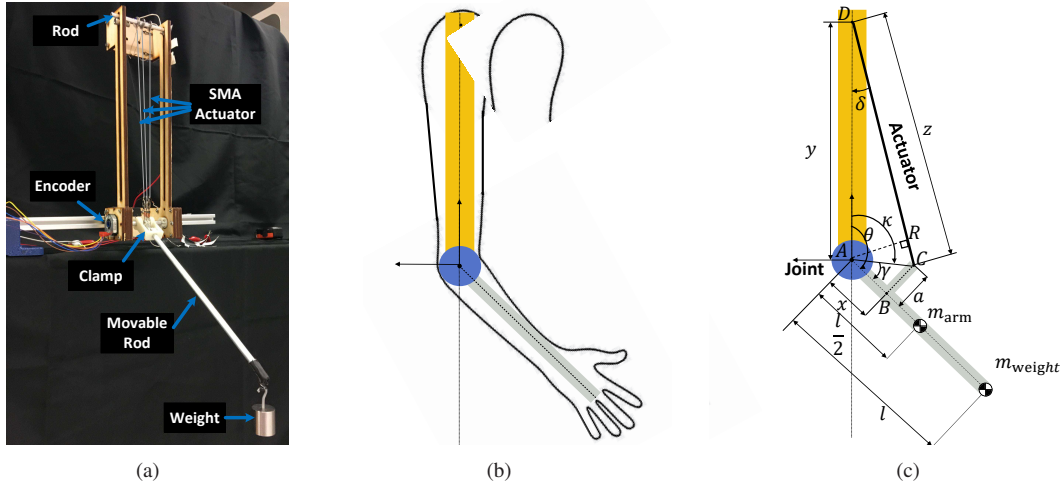


Fig. 5. (a). The experimental setup for the robotic bicep system. (b). A schematic of the human bicep-forearm system. (c). Illustration of the robotic bicep for quasi-static analysis.

TABLE I
MODELING, VERIFICATION, AND CONTROL PERFORMANCE FOR THE SMA ACTUATOR AND SMA-ACTUATED ROBOTIC BICEP

	Average error proposed	Average error linear	Standard deviation proposed	Standard deviation linear
$F - q(T)$ identification	0.8%	2.2%	0.8%	1.7%
$F - q(T)$ verification	0.9%	2.7%	0.7%	1.7%
$F - q(T)$ compensation	1.3%	2.1%	0.8%	1.5%
$L - q(T)$ identification	2.9%	14.1%	3.4%	9.9%
$L - q(T)$ verification	3.4%	12.6%	5.2%	9.9%
$L - q(T)$ compensation	4.9%	11.5%	5.5%	9.5%
Robot control (sinusoidal)	1.8°	3.4°	0.8°	1.7°
Robot control (random)	1.6°	4.2°	1.1°	2.9°

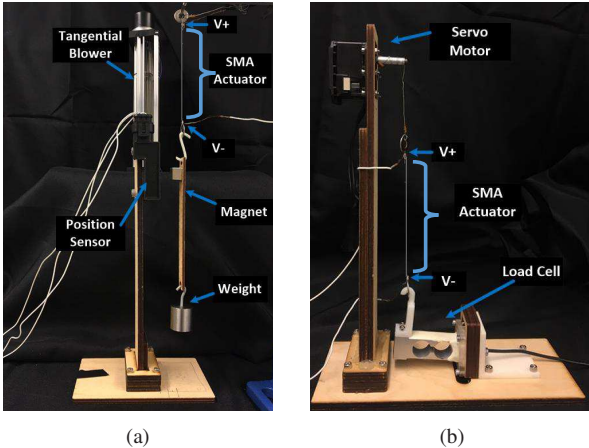


Fig. 6. The experimental setup for (a) $L - q(T)$ hysteresis, and (b) $L - F$ and $F - q(T)$ hysteresis measurements of an SMA actuator.

with a metal rod at the top for connecting one end of the SMA actuators, and symmetric bearing assemblies (602ZZ, VXB) at the bottom of the structure to house a rotating shaft. A 3D printed connector (M200, Zortrax) attached an 8 mm diameter, 30 cm long aluminum rod perpendicularly to the shaft, and a capacitive quadrature encoder (AMT103, CUI) was mounted on the bottom outer structure to measure the shaft rotation with an accuracy of 0.176° . The aluminum rod

acted as the movable link, and featured a 3D printed clamp for easy connection to the other end of the SMA actuators. The weight of the rod was 40 g. A fan was used for even airflow environment and was not shown in Fig. 5(a). The clamp and top metal rod were tightened in place for a rigid connection between the arm structure and the SMA actuators. A 100 g weight was hung from the end of the actuated link. The system was designed to mimic a human bicep-forearm system lifting a weight through some angles of rotation (Fig. 5(b)), and was developed such that the SMA actuator connection points can be easily modified.

It was noted that the lengths of the three SMA actuators were all close to 27 cm. This would allow us to assume an equal performance of each actuator, and the identified model and control algorithm in this study could be directly employed. Three SMA actuators were utilized to increase the amount of weight that could be lifted by the robotic bicep. Although the adopted SMA actuators exhibited similar properties, the small length difference among the actuators was likely to cause certain modeling and control discrepancies.

VII. RESULTS

A. Performance Metric

The performance was measured by the average absolute errors and the standard deviation divided by the corresponding output range:

$$E_{\text{average}} = \frac{\sum_{i=1}^M |e_i|/M}{P} \times 100\%, \quad (23)$$

$$\sigma = \frac{\sqrt{\sum_{i=1}^M (e_i - \bar{e})^2}}{P} \times 100\%, \quad (24)$$

where M was the number of data-points to be evaluated, e_i denoted the error of the i_{th} point, P was the output range, and \bar{e} was the average error. They were denoted as the average error and the standard deviation percentages.

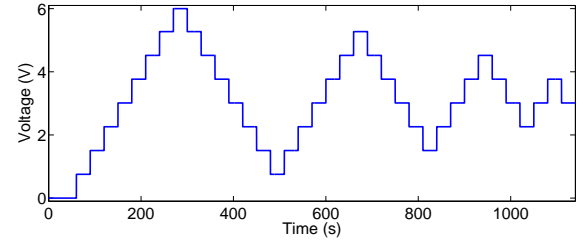
In this paper, we consider the quasi-static relationships, which is based on the steady-state values after transient process, so the specific time information is irrelevant. Instead, the term ‘‘index’’ refers to the numbering of the quasi-static voltage, contraction length, and tension force values.

B. Model Identification

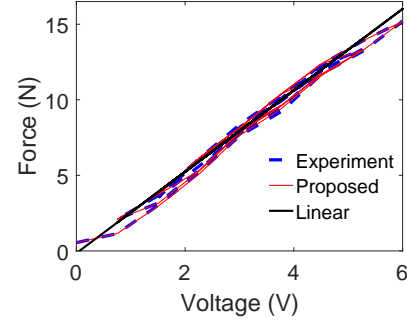
To obtain the experimental $F - q(T)$ hysteresis and $L - q(T)$ hysteresis, the voltage input was chosen to be in the form of damped oscillations (Fig. 7(a)) [23], [31]. Under resting length condition, the $F - q(T)$ hysteresis was obtained. The $L - q(T)$ hysteresis under different tension forces was also measured (Fig. 3). The discretization levels of the Preisach models H_1 and H_2 , N_1 and N_2 , were empirically chosen to be 10 and 20, respectively, since the resulted model is accurate but not over complicated. Further increasing N_1 and N_2 did not produce substantial improvement in modeling accuracy, but would further complicate the model.

H_1 was identified based on the $F - q(T)$ hysteresis. Fig. 7(b) shows that the proposed model could accurately capture the $F - q(T)$ hysteresis. Fig. 7(c) and Fig. 8(d) shows the modeling error results. A total of 37 data points were employed for the modeling error analysis. The average error and standard deviation percentages were 0.8% and 0.8%, respectively, as shown in Table I. It was identified that the constant term $c_0 = 7.89$ N, and the model parameters were shown in Fig. 8(a) (left): Since the $F - q(T)$ hysteresis was mild, the identified parameters of the Preisach model H_1 were primarily located close to the $\beta = \alpha$ line. While this indeed meant that a linear model could be used, it would be shown later that the adoption of a hysteresis model still delivered considerably more improved accuracy.

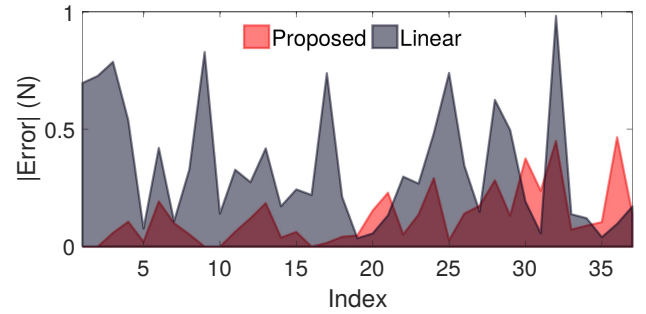
H_2 was identified based on the $L - q(T)$ hysteresis and the identified H_1 . The modeling performance was shown in Fig. 8(b)-(d). Since 37 different voltage steps were applied to the actuator under each tension condition, and four tension conditions were tested, a total of 148 data points were employed for the analysis. The average modeling error and standard deviation percentages were calculated as 2.9% and 3.4%, respectively (Table I). The hysteresis saturated at high temperatures (Fig. 3(b)) and was captured by the model. The model parameters were provided in Fig. 8(a) (right), and the constant term $c_1 = 1.39$ mm. The parameters of H_2 were small at high α and β values, contributing to the saturating profile. Since the $L - q(T)$ hysteresis was significant, a considerable



(a)



(b)



(c)

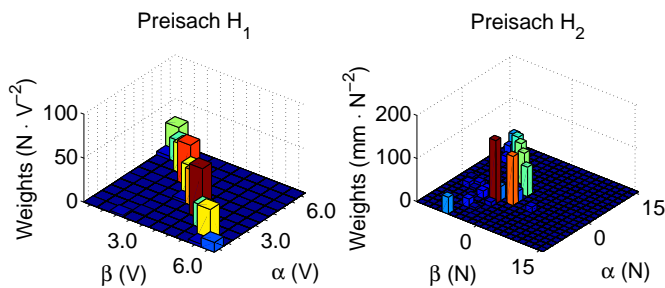
Fig. 7. (a). The voltage steps input. (b). Modeling performances and (c) modeling error comparisons with the proposed model and the linear model of the $F - q(T)$ hysteresis.

number of model parameters were located away from the $\beta = \alpha$ line.

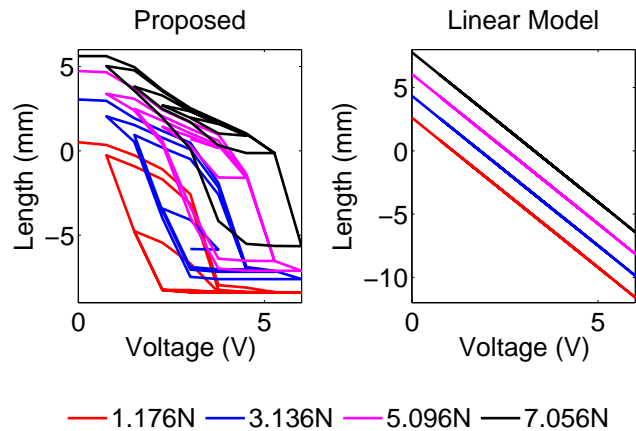
The average time for each contraction length calculation was 0.78 ms. The computations were run in MATLAB software on a desktop HP 280 G1 MT with Intel(R) Pentium(R) G3260 CPU at 3.30 GHz and 12 GB memory.

C. Model Comparison

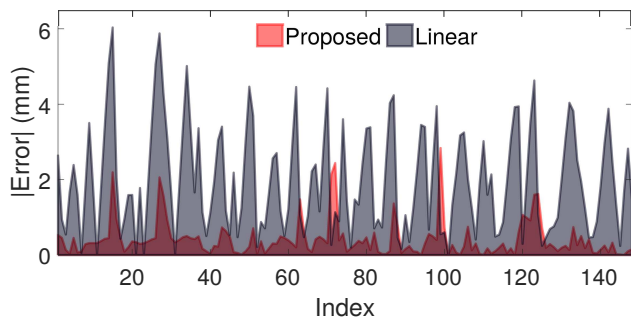
For comparison purposes, a linear model was also realized. The parameters of the linear model were identified as $k_1 = 2.69$ N/V, $k_2 = 0.88$ mm/V and $F_0 = -0.15$ N. As can be seen, the identified pre-tension (F_0) was not accurate since the applied pre-tension value was 0.5 N. The modeling performance of the $F - q(T)$ hysteresis was obtained (Fig. 7(b)-(c) and Fig. 8(d)), and the modeling performance of the $L - q(T)$ hysteresis was calculated (Fig. 8(b)-(d)). The average errors and standard deviations for the $F - q(T)$ hysteresis and the $L - q(T)$ hysteresis were presented (Table I). The linear model produced about 160% larger error than that of the proposed model for the $F - q(T)$ hysteresis, and around 300% larger error than that



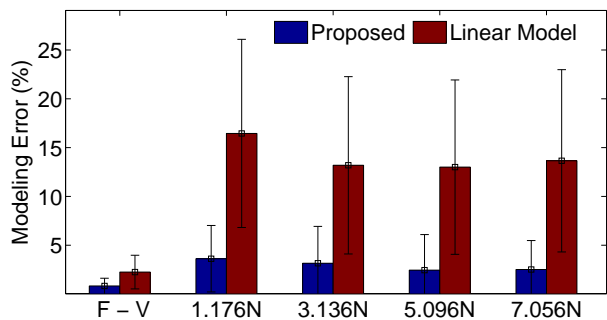
(a)



(b)



(c)



(d)

Fig. 8. (a). The identified parameters of the Preisach model H_1 (left) and H_2 (right). (b). Modeling performance with the proposed model (left) and the linear model (right). (c). Modeling error comparison for the $L-q(T)$ hysteresis. (d). The modeling error comparison for the $F-q(T)$ hysteresis and $L-q(T)$ hysteresis with the proposed model and the linear model.

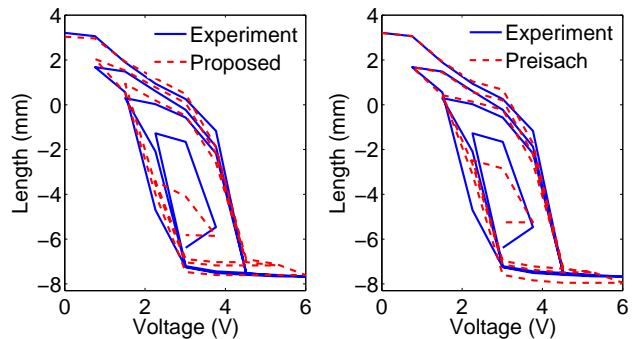


Fig. 9. Modeling results of the $L-q(T)$ hysteresis under $F = 3.136$ N with the proposed model (left) and a two-dimensional Preisach Model (right).

of the proposed model for the $L-q(T)$ hysteresis. The average time for each contraction length calculation was 0.07 ms. Although the computation of this approach was more efficient than that of the proposed model, its modeling performance was much worse.

The comparison between the proposed model and an existing two-dimensional hysteresis model was then conducted. Since two-dimensional hysteresis models could not be directly employed to characterize three-dimensional hysteresis, we only considered a special case – the $L-q(T)$ hysteresis when the tension force was held at 3.136 N. A conventional two-dimensional Preisach model was identified and compared with the proposed model, as shown in Fig. 9. The discretization level of the Preisach model was also chosen to be 20 for a fair comparison. The average errors of the proposed model and the Preisach model were 0.44 mm and 0.33 mm, respectively. The standard deviations of the proposed model and the Preisach model were 0.53 mm and 0.37 mm, respectively. Although the Preisach model produced approximately 30% less error than the proposed model, it could not work for three-dimensional cases where the tension force also changed. While more detailed comparisons with other existing two-dimensional hysteresis models were not provided in this study, the comparison of those models could be found in [32], [38].

The proposed approach was further tested and compared with a linear model for characterizing the hysteresis in other popular robotic artificial muscles. The McKibben actuators and SCP actuators exhibited coupled hysteresis. Fig. 10(a)-(c) shows the hysteresis in a McKibben actuator between Force, Pressure, and Length [18]. The discretization levels of the Preisach models H_1 and H_2 , N_1 and N_2 , were both chosen to be 20. It was confirmed that the proposed model could successfully capture the three-dimensional hysteresis in the McKibben actuator, as shown in Fig. 10(g). Since the Force – Pressure relationship was approximately linear, both approaches had good performance for modeling Force – Pressure hysteresis. Fig. 10(d)-(f) shows the hysteresis in an SCP actuator between Force, Voltage, and Length [22], [23]. The discretization levels of the Preisach models H_1 and H_2 , N_1 and N_2 , were chosen to be 10 and 20, respectively. The modeling results are provided in Fig. 10(h). The effectiveness of the proposed model was further validated.

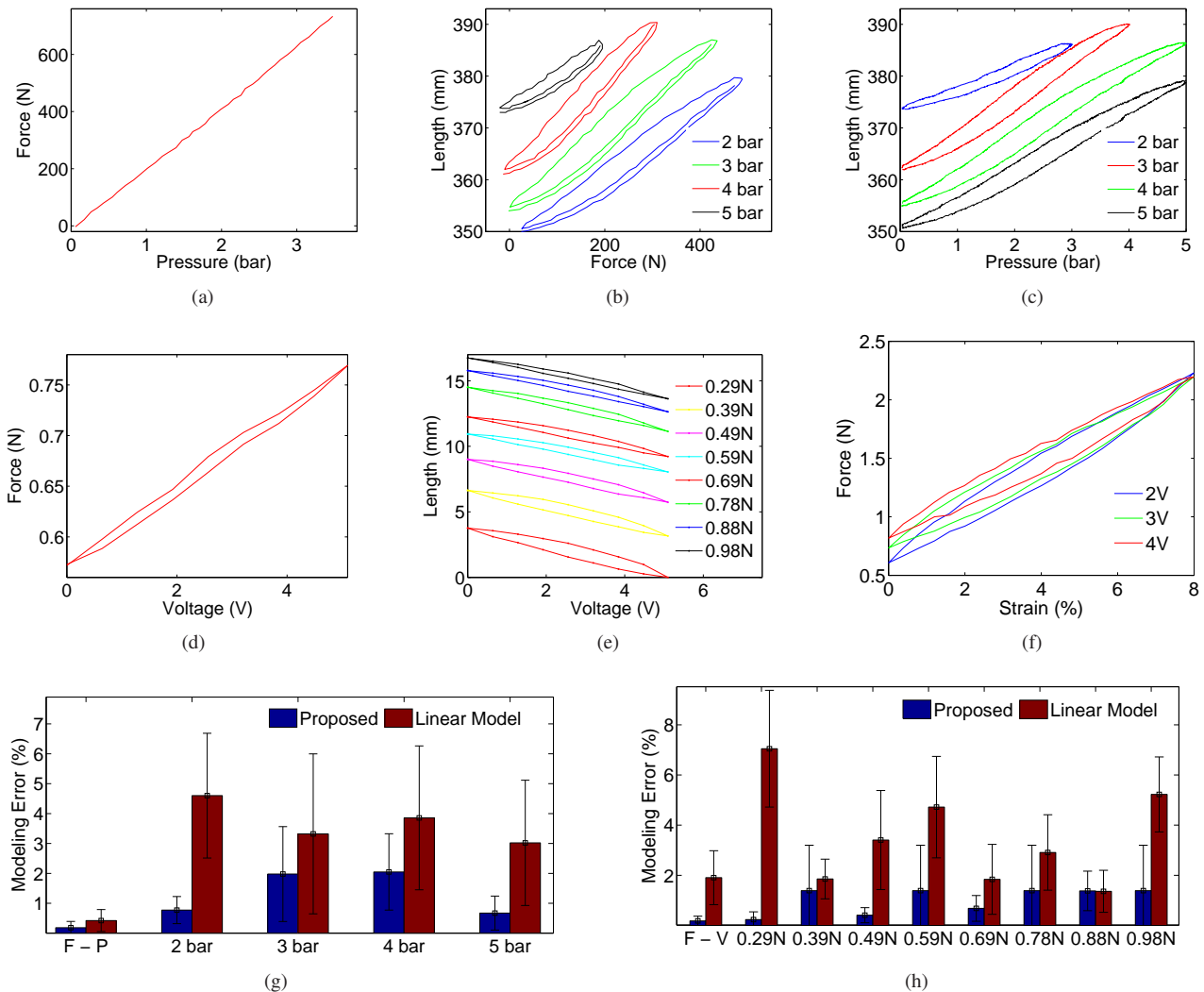


Fig. 10. Three-dimensional hysteresis in a McKibben actuator between the (a) Force – Pressure, (b) Length – Force, and (c) Length – Pressure hysteresis. The data was from [18] and obtained by an online web plot digitizer (<http://arohatgi.info/WebPlotDigitizer/>). Since the Length – Pressure hysteresis was obtained from two serially connected actuators, this hysteresis was provided here only for illustration purposes. Three-dimensional hysteresis in an SCP actuator between the (d) Force – Voltage, (e) Length – Voltage, and (g) Force – Length hysteresis. It was found in experiment that the $F - q(T)$ hysteresis was mild and the magnitude was dependent on the pre-tension force. The modeling error comparison results were provided for the (g) McKibben actuator and the (h) SCP actuator.

D. Model Verification

The model identification results showed that the proposed model could effectively capture the three-dimensional hysteresis in the SMA actuator under the damped-oscillation voltage input. To confirm that the model could reliably estimate tension force and contraction length under any reasonable inputs, additional experiments utilizing random inputs were conducted.

To verify the model for the $F - q(T)$ hysteresis, a randomly-chosen voltage input (Fig. 11(a)) consisting of 74 different steps was applied to the SMA actuator when the actuator was close to resting length. The experimental measurements of the steady-state force values were obtained (Fig. 11(b)). Fig. 11(c) shows the force estimation errors under the proposed model and the linear model. The model verification for the $L - q(T)$ hysteresis was also conducted. A different random

voltage steps input (Fig. 12(a)) was applied to the actuator under different tension forces. The experimental measurements of the steady-state contraction length values were obtained (Fig. 12(b)), and each data point was obtained from a single trial under a constant tension condition. Since 51 different voltage steps were applied to the actuator under each tension condition, and four tension conditions were tested, a total of 204 samples were adopted for analysis. Fig. 12(c) shows the contraction length estimation errors under the proposed model and the linear model. The corresponding average estimation errors and standard deviations were summarized (Table I). The proposed model produced more accurate estimations than the linear model.

E. Inverse Compensation

The inverse compensation was first examined in feedforward force control. The reference force sequence was chosen to

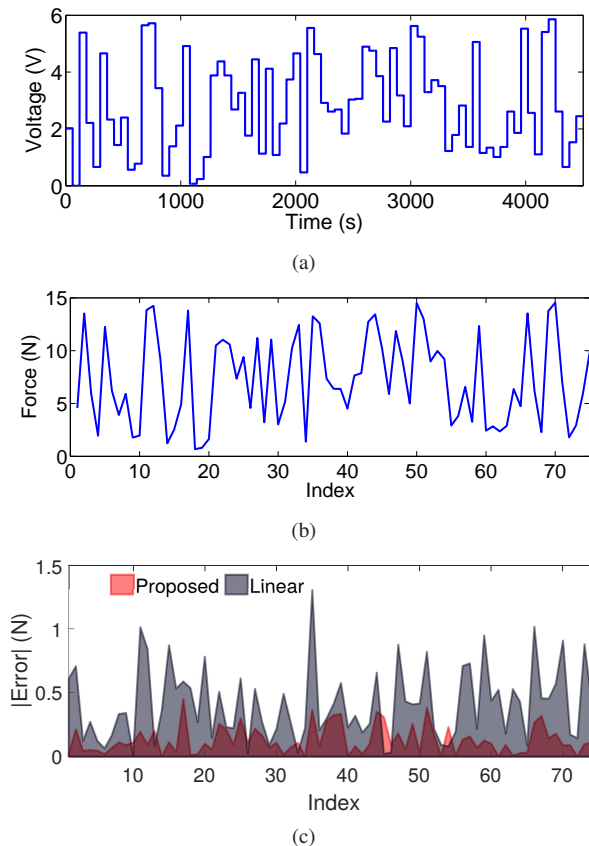


Fig. 11. (a). A random voltage steps input for model verification. (b). The corresponding steady-state tension force measurements. (c). Errors in tension force predictions based on the proposed model and the linear model.

be a series of random profiles (Fig. 13(a)). Corresponding temperature surrogate (voltage step) inputs were computed off-line based on the inverse algorithms of the proposed model and the linear model, and then applied to the actuator. The control errors were calculated based on 74 force control results (Table I and Fig. 13(b)). The proposed scheme outperformed the linear model inverse method. The inverse compensation was further examined in contraction length control. Similarly, the reference contraction length sequence was chosen to be a series of random profiles (Fig. 13(c)). Corresponding temperature surrogate input values were computed. Since 30 different voltage steps were applied to the actuator under each tension condition, and four tension conditions were tested, a total of 120 control steps were adopted. The control errors of the proposed approach and the linear model inverse were obtained (Table I and Fig. 13(d)). The effectiveness of the proposed compensation method was evident.

The proposed method was compared with existing studies on control of robotic artificial muscles. It was found that the control accuracy of the proposed compensation algorithm was not higher than existing methods. This can be explained as follows: Firstly, a predominant class of the existing studies focused on two-dimensional hysteresis while holding the third-dimensional property as a constant [11]–[13], [18]. Although accurate characterization and compensation were achieved, these models could not work for many practical cases where

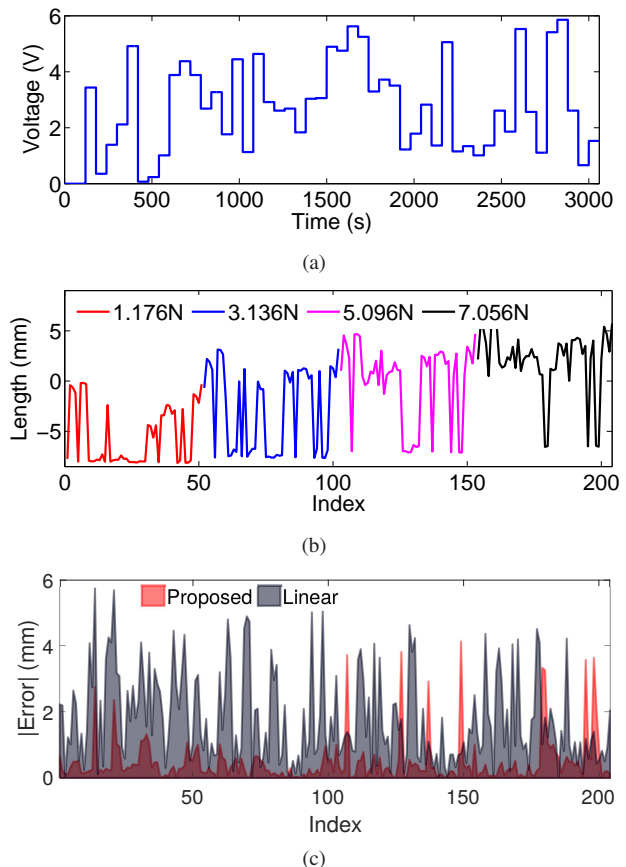


Fig. 12. (a). A random voltage steps input for model verification. (b). The experimental steady-state contraction length measurements under different tension forces. (c). Errors in contraction length predictions based on the proposed model and the linear model.

the third-dimensional property also changes. This study proposed an approach that can capture and compensate for the three-dimensional hysteresis. The computational cost of the proposed method is comparable to that of the two-dimensional hysteresis compensation. Secondly, most of the existing studies adopted feedback controls [12], [13], [22], [47], where the input to the system was updated in real-time by comparing the desired output and the current status of the system. The realization of feedback control required additional sensing equipment, which was often undesirable considering the cost and complexity. The proposed method was a feedforward control strategy that required no sensing equipment.

F. Robotic Bicep

The feedforward control of the robotic bicep was demonstrated. The operating range was calculated to be 47.5° based on the system configuration, and experimentally verified by measuring the arm's maximum moving angle range under no voltage and the peak voltage. We considered the quasi-static angle control of the robotic bicep. The dynamics of the SMA actuators and robotic bicep have been explored in existing literature [9], [16] and the control of the dynamical system is one of the future directions of this study.

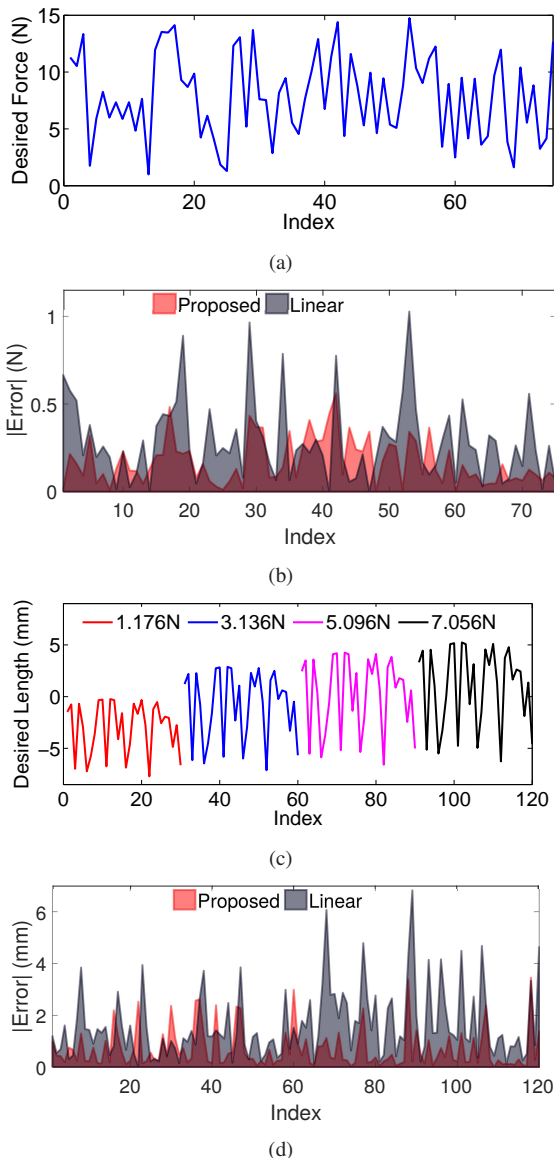


Fig. 13. (a). A randomly chosen reference force sequence. (b). Inverse compensation results for $F - q(T)$ hysteresis with the proposed inverse compensation and the linear model inverse. (c). A randomly chosen reference contraction length sequence. (d). Inverse compensation results for $L - q(T)$ hysteresis with the proposed approach and the linear method.

Experiments were conducted to examine the feedforward control performance. To achieve an equilibrium angle θ_d , the corresponding contraction length L_d and tension force F_d of the actuators were calculated. The required voltage steps were then computed based on the proposed model inverse and the linear model inverse, respectively. Similarly, each voltage step was also held for 30 s. The speed of the robotic bicep movement depended on the dynamics of the SMA actuators. Under each voltage step, the majority portion of the bicep movement was completed within 3 s in this study.

The reference angle sequence was chosen to be a sinusoidal profile consisting of 40 values (Fig. 14(a)). The corresponding tension force and contraction length values were calculated. Two voltage step sequences were obtained based on the inverse

algorithms for the proposed model and the linear model, respectively. The control performance was shown (Fig. 14(b) and Table I). The linear model-based controller produced around 90% larger errors than the proposed strategy. Furthermore, the reference angle sequence was chosen to be a random profile (Fig. 14(c)). The control performance was provided (Fig. 14(d) and Table I). The effectiveness of the proposed scheme was further validated.

VIII. CONCLUSION AND DISCUSSION

In this study, we proposed a methodology to capture the three-dimensional hysteresis in different robotic artificial muscles by recursively embedding two Preisach models. We showed that modeling and inverting the proposed model allowed us to drive the SMA actuators to generate designed contraction length and tension force. To show its use in practice, feedforward control of an SMA-actuated one-link robotic bicep was demonstrated, where strain and tension force of the SMA actuators varied continuously. This work can be applied to many relevant studies and is generalizable in the following aspects:

Any existing two-dimensional hysteresis models can be adopted as the embedding element to construct the proposed model. Although the Preisach model was utilized in this study because of its proven effectiveness, the proposed scheme was not constrained to any hysteresis models. This has great practical usages since different embedding elements can be chosen based on different applications. In cases where control accuracy is more important than computational and storage costs, the Preisach model with a large number of model parameters can be utilized; in cases where efficient implementation is more desirable, other hysteresis models that have simpler model structures can be employed, such as the Prandtl-Ishlinskii model and the Bouc-Wen model. More discussions on the properties and comparisons of the existing hysteresis models can be found in [32], [38].

The proposed model is a phenomenological approach. The model derivation is independent of material's physical properties. When the values of the model parameters change, the model can capture different hysteresis behaviors. This is why the proposed methodology works for SMA actuators with other diameters and materials, as well as other types of robotic artificial muscles, such as the McKibben actuators, SCP actuators, and ionic polymer-metal composite (IPMC) artificial muscles [48], [49]; preliminary results are provided in Fig. 10(g)-(h). Note that other robotic artificial muscles might have alternative hysteretic elements. For example, for IPMC artificial muscles, the hysteresis variables are stress, bending displacement, and voltage. Furthermore, the proposed study can be generalized to compensate for the hysteresis in a broad range of robotic artificial muscles since the compensation can be realized by inverting the corresponding hysteresis model. Like other phenomenological models, the model parameters need to be identified for a particular system with experiments. By utilizing the relationship between the hysteresis profile and other actuator specifications (e.g., material, diameter, fatigue, and length), the number of required experiments can be

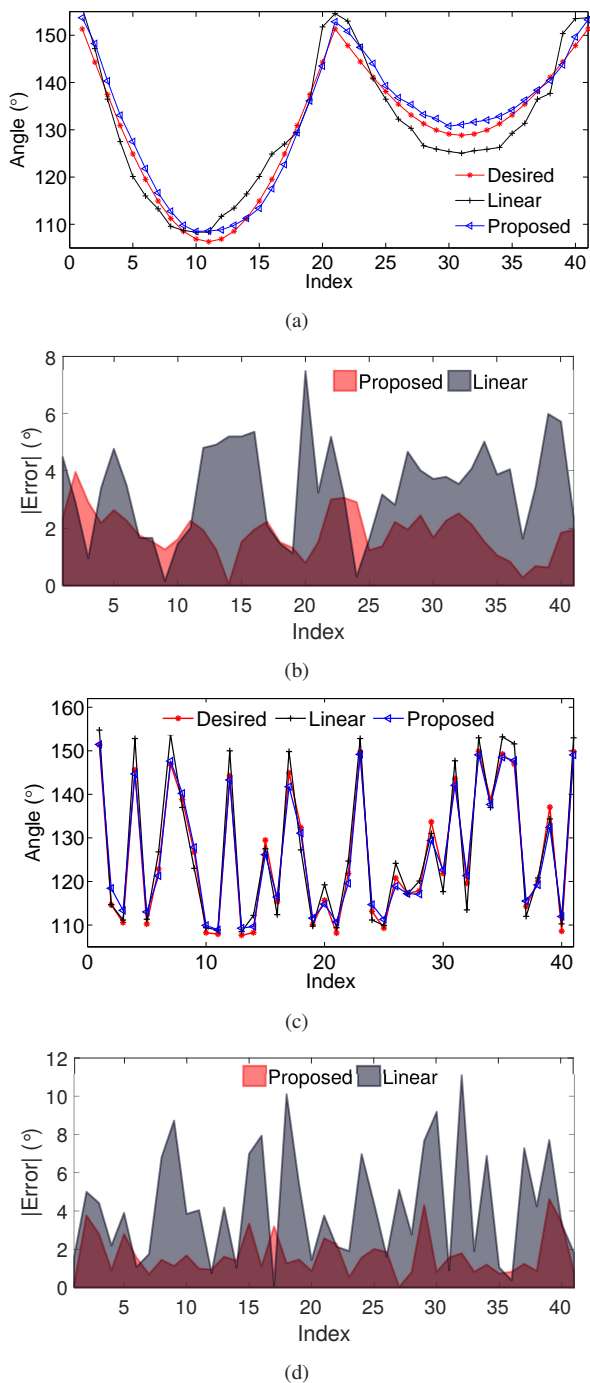


Fig. 14. Robotic bicep angle control results. (a). A sinusoidal-profile reference angle sequence and corresponding control performance. (b). Corresponding angle control errors with the proposed inverse compensation and the inverse of the linear model. (c). A random-profile reference angle sequence and the corresponding control performance. (d). Corresponding control errors with the proposed inverse compensation and the inverse of the linear model.

reduced. For example, SMA actuators with the same diameter and temperature but with different lengths can often generate the same strain [5], so no additional experiments are needed if the strain is of interest.

Our method is able to describe higher-dimensional coupled hysteresis beyond three dimensions. Multi-dimensional hysteresis with coupled inputs can be constructed by embedding

a multi-stage hysteresis model. To illustrate the idea, denote T_i , $i = 1, 2, \dots, N-1$, as hysteresis models, Y as the output, and X_1, X_2, \dots, X_{N-1} as inputs that are coupled. First, model the hysteresis between X_1 and X_2 as $X_2 = T_1[X_1]$. By embedding T_1 , a three-dimensional model is obtained: $X_3 = T_2[X_2 - T_1[X_1]]$. An N -dimensional hysteresis model can be obtained through further embedding:

$$Y = T_{N-1}[X_{N-1} - T_{N-2}[X_{N-2} - \dots - T_2[X_2 - T_1[X_1]] \dots]. \quad (25)$$

Unlike several existing multi-dimensional hysteresis models that considered independent input variables [41], [42], this model can describe coupled hysteresis between input variables. The proposed model is also different from [43], [44] in that the formulation of the proposed model is not constrained to be additive. While only the detailed analysis of the three-dimensional case is provided, the proposed method may also apply to higher-dimensional scenarios.

Several future areas of development can be considered:

This study considered the quasi-static hysteresis and the steady-state performance, the analysis including the system dynamics will be considered. In dynamical systems, the quasi-static hysteretic relationships may or may not hold, depending on whether there is rate-dependent hysteresis or not. For rate-independent hysteretic systems, system properties can be described well by jointly considering the system dynamics and the static hysteresis. For example, for SMA actuators, the thermal dynamics between the voltage and temperature, expressed in Eq. (1), should be considered. For rate-dependent hysteretic systems, additional dimensions to the hysteresis modeling will need to be added.

Our method used voltage as a surrogate variable to infer temperature, and the study with actual temperature measurements in real environments will be studied. The temperature of SMA actuators is dependent on the actuator's properties and the ambient environmental conditions, such as the ambient temperature and air flow. By conducting additional experiments to estimate the thermal dynamics properties, the relationship between voltage and temperature of the actuator can be obtained. It may also be of interest to use a dedicated thermal imaging device for accurate temperature measurement. Although the proposed study can effectively compensate for the hysteresis, remaining errors still exist. In cases where feedback control is possible, the proposed feedforward control strategy can be used in conjunction with feedback control to further reduce the uncompensated errors and achieve desirable control performances.

ACKNOWLEDGMENTS

We thank members of the Advanced Robotics and Controls Lab at University of California San Diego for intellectual discussions and technical help. We thank the Bioinspired Robotics and Design Lab directed by Michael T. Tolley at University of California San Diego for providing the image of the McKibben actuator (Fig. 1(b)).

REFERENCES

- [1] B. Tondu, "What is an artificial muscle? A systemic approach," *Actuators*, vol. 4, no. 4, pp. 336–352, 2015.
- [2] R. H. Baughman, "Playing nature's game with artificial muscles," *Science*, vol. 308, no. 5718, pp. 63–65, 2005.
- [3] R. V. Ham, T. G. Sugar, B. Vanderborght, K. W. Hollander, and D. Lefeber, "Compliant actuator designs," *IEEE Robot. Autom. Mag.*, vol. 16, no. 3, pp. 81–94, 2009.
- [4] J. Zhang and M. C. Yip, "Three-dimensional hysteresis modeling of robotic artificial muscles with application to shape memory alloy actuators," in *Proceedings of Robotics: Science and Systems (RSS) XIII*, 2017.
- [5] J. M. Jani, M. Leary, A. Subic, and M. A. Gibson, "A review of shape memory alloy research, applications and opportunities," *Materials & Design*, vol. 56, pp. 1078–1113, 2014.
- [6] S. Seok, C. D. Onal, K. J. Cho, R. J. Wood, D. Rus, and S. Kim, "Meshworm: A peristaltic soft robot with antagonistic nickel titanium coil actuators," *IEEE/ASME Tran. Mech.*, vol. 18, no. 5, pp. 1485–1497, 2013.
- [7] F. Simone, G. Rizzello, and S. Seelecke, "Metal muscles and nerves – a self-sensing SMA-actuated hand concept," *Smart Mater. Struct.*, vol. 26, no. 9, p. 095007, 2017.
- [8] Z. Zhakypov, J. L. Huang, and J. Paik, "A novel torsional shape memory alloy actuator: Modeling, characterization, and control," *IEEE Robot. Autom. Mag.*, vol. 23, no. 3, pp. 65–74, 2016.
- [9] J. Sheng and J. P. Desai, "Design, modeling and characterization of a novel meso-scale SMA-actuated torsion actuator," *Smart Mater. Struct.*, vol. 24, no. 10, p. 105005, 2015.
- [10] C. Cisse, W. Zaki, and T. B. Zineb, "A review of constitutive models and modeling techniques for shape memory alloys," *Int. J. Plasticity*, vol. 76, pp. 244–284, 2016.
- [11] D. Hughes and J. T. Wen, "Preisach modeling of piezoceramic and shape memory alloy hysteresis," *Smart Mater. Struct.*, vol. 6, no. 3, p. 287, 1997.
- [12] A. Kilicarslan, G. Song, and K. Grigoriadis, "Modeling and hysteresis compensation in a thin SMA wire using ANFIS methods," *J. Intell. Mater. Syst. Struct.*, vol. 22, no. 1, pp. 45–57, 2011.
- [13] M. R. Zakerzadeh and H. Sayyaadi, "Precise position control of shape memory alloy actuator using inverse hysteresis model and model reference adaptive control system," *Mechatronics*, vol. 23, no. 8, pp. 1150–1162, 2013.
- [14] C.-P. Chou and B. Hannaford, "Measurement and modeling of McKibben pneumatic artificial muscles," *IEEE Trans. Robot. Autom.*, vol. 12, no. 1, pp. 90–102, 1996.
- [15] Y.-L. Park, B. rong Chen, N. O. Perez-Arancibia, D. Young, L. Stirling, R. J. Wood, E. C. Goldfield, and R. Nagpal, "Design and control of a bio-inspired soft wearable robotic device for ankle-foot rehabilitation," *Bioinspir. Biomim.*, vol. 9, no. 1, p. 016007, 2014.
- [16] A. Hosovsky, J. Pitel, K. Zidek, M. Tothova, J. Sarosi, and L. Cveticanin, "Dynamic characterization and simulation of two-link soft robot arm with pneumatic muscles," *Mech. Mach. Theory*, vol. 103, pp. 98–116, 2016.
- [17] S. A. DeLaHunt, T. E. Pillsbury, and N. M. Wereley, "Variable recruitment in bundles of miniature pneumatic artificial muscles," *Bioinspir. Biomim.*, vol. 11, no. 5, p. 056014, 2016.
- [18] C.-J. Lin, C.-R. Lin, S.-K. Yu, and C.-T. Chen, "Hysteresis modeling and tracking control for a dual pneumatic artificial muscle system using Prandtl-Ishlinskii model," *Mechatronics*, vol. 28, pp. 35–45, 2015.
- [19] T. Vo-Minh, T. Tjahjowidodo, H. Ramon, and H. V. Brussel, "A new approach to modeling hysteresis in a pneumatic artificial muscle using the Maxwell-slip model," *IEEE/ASME Trans. Mech.*, vol. 16, no. 1, pp. 177–186, 2011.
- [20] M. D. Lima, N. Li, M. Jung de Andrade, S. Fang, J. Oh, G. M. Spinks, M. E. Kozlov, C. S. Haines, D. Suh, J. Foroughi, S. J. Kim, Y. Chen, T. Ware, M. K. Shin, L. D. Machado, A. F. Fonseca, J. D. W. Madden, W. E. Voit, D. S. Galvão, and R. H. Baughman, "Electrically, chemically, and photonically powered torsional and tensile actuation of hybrid carbon nanotube yarn muscles," *Science*, vol. 338, no. 6109, pp. 928–932, 2012.
- [21] C. S. Haines, M. D. Lima, N. Li, G. M. Spinks, J. Foroughi, J. D. W. Madden, S. H. Kim, S. Fang, M. Jung de Andrade, F. Göktepe, Ö. Göktepe, S. M. Mirvakili, S. Naficy, X. Lepró, J. Oh, M. E. Kozlov, S. J. Kim, X. Xu, B. J. Swedlove, G. G. Wallace, and R. H. Baughman, "Artificial muscles from fishing line and sewing thread," *Science*, vol. 343, no. 6173, pp. 868–872, 2014.
- [22] M. C. Yip and G. Niemeyer, "On the control and properties of super-coiled polymer artificial muscles," *IEEE Trans. Robot.*, vol. 33, no. 3, pp. 689–699, 2017.
- [23] J. Zhang, K. Iyer, A. Simeonov, and M. C. Yip, "Modeling and inverse compensation of hysteresis in super-coiled polymer artificial muscles," *IEEE Robot. Autom. Lett.*, vol. 2, no. 2, pp. 773–780, 2017.
- [24] S. Y. Yang, K. H. Cho, Y. Kim, M.-G. Song, H. S. Jung, J. W. Yoo, H. Moon, J. C. Koo, J. do Nam, and H. R. Choi, "High performance twisted and coiled soft actuator with spandex fiber for artificial muscles," *Smart Mater. Struct.*, vol. 26, no. 10, p. 105025, 2017.
- [25] F. Karami and Y. Tadesse, "Modeling of twisted and coiled polymer (TCP) muscle based on phenomenological approach," *Smart Mater. Struct.*, 2017, to appear.
- [26] Q. Yang and G. Li, "A top-down multi-scale modeling for actuation response of polymeric artificial muscles," *J. Mech. Phy. Solids*, vol. 92, pp. 237–259, 2016.
- [27] C. Xiang, H. Yang, Z. Sun, B. Xue, L. Hao, M. D. A. Rahoman, and S. Davis, "The design, hysteresis modeling and control of a novel SMA-fishing-line actuator," *Smart Mater. Struct.*, vol. 26, no. 3, p. 037004, 2017.
- [28] D. Jiles and D. Atherton, "Theory of ferromagnetic hysteresis," *J. Magn. Magn. Mater.*, vol. 61, no. 1, pp. 48–60, 1986.
- [29] D. Habineza, M. Rakotondrabe, and Y. Le Gorrec, "Bouc-Wen modeling and feedforward control of multivariable hysteresis in piezoelectric systems: Application to a 3-DoF piezotube scanner," *IEEE Trans. Contr. Syst. T.*, vol. 23, no. 5, pp. 1797–1806, 2015.
- [30] G. Y. Gu, C. X. Li, L. M. Zhu, and C. Y. Su, "Modeling and identification of piezoelectric-actuated stages cascading hysteresis nonlinearity with linear dynamics," *IEEE/ASME Trans. Mech.*, vol. 21, no. 3, pp. 1792–1797, 2016.
- [31] X. Tan and J. Baras, "Modeling and control of hysteresis in magnetostrictive actuators," *Automatica*, vol. 40, no. 9, pp. 1469–1480, 2004.
- [32] I. Mayergoyz, *Mathematical models of hysteresis*. Springer-Verlag, 1991.
- [33] Z. Sun, L. Hao, B. Song, R. Yang, R. Cao, and Y. Cheng, "Periodic reference tracking control approach for smart material actuators with complex hysteretic characteristics," *Smart Mater. Struct.*, vol. 25, no. 10, p. 105029, 2016.
- [34] L. Shu, G. Wu, D. Chen, and M. J. Dapino, "Modeling of galfenol bending actuator considering nonlinear hysteresis and dynamic real-time control strategy," *Smart Mater. Struct.*, vol. 25, no. 3, p. 035046, 2016.
- [35] J. Zhang, E. Merced, N. Sepúlveda, and X. Tan, "Modeling and inverse compensation of non-monotonic hysteresis in VO₂-coated microactuators," *IEEE/ASME Trans. Mech.*, vol. 19, no. 2, pp. 579–588, 2014.
- [36] M. Al Janaideh, S. Rakheja, and C.-Y. Su, "An analytical generalized Prandtl-Ishlinskii model inversion for hysteresis compensation in micro-positioning control," *IEEE/ASME Tran. Mech.*, vol. 16, no. 4, pp. 734–744, 2011.
- [37] K. K. Leang, Q. Zou, and S. Devasia, "Feedforward control of piezoactuators in atomic force microscope systems," *IEEE Control Systems*, vol. 29, no. 1, pp. 70–82, 2009.
- [38] J. Zhang, D. Torres, J. Ebel, N. Sepúlveda, and X. Tan, "A composite hysteresis model in self-sensing feedback control of fully integrated VO₂ microactuators," *IEEE/ASME Trans. Mech.*, vol. 21, no. 5, pp. 2405–2417, 2016.
- [39] O. Aljanaideh, S. Rakheja, and C.-Y. Su, "Experimental characterization and modeling of rate-dependent asymmetric hysteresis of magnetostrictive actuators," *Smart Mater. Struct.*, vol. 23, no. 3, p. 035002, 2014.
- [40] R. Oubellil, L. Ryba, A. Voda, and M. Rakotondrabe, "Experimental model inverse-based hysteresis compensation on a piezoelectric actuator," in *International Conference on System Theory, Control and Computing*, 2015, pp. 186–191.
- [41] G. Finocchio, E. Cardelli, and B. Azzzerboni, "A simplified model for vector hysteresis computation," *IEEE Trans. Magn.*, vol. 42, no. 4, pp. 955–958, 2006.
- [42] P. Krejci and J. Sprekels, "On a class of multi-dimensional Prandtl-Ishlinskii operators," *Physica B: Condensed Matter*, vol. 306, no. 14, pp. 185–190, 2001.
- [43] M. Rakotondrabe, "Multivariable classical Prandtl-Ishlinskii hysteresis modeling and compensation and sensorless control of a nonlinear 2-dof piezoactuator," *Nonlinear Dynamics*, pp. 1–19, 2017.
- [44] Z. Li and J. Shan, "Modeling and inverse compensation for coupled hysteresis in piezo-actuated fabry-perot spectrometer," *IEEE/ASME Tran. Mech.*, vol. 22, no. 4, pp. 1903–1913, 2017.
- [45] D. Leo, *Engineering analysis of smart material systems*, ser. Wiley InterScience. Wiley, 2007.

- [46] T. Wang, Z. Shi, D. Liu, C. Ma, and Z. Zhang, "An accurately controlled antagonistic shape memory alloy actuator with self-sensing," *Sensors*, vol. 12, no. 6, p. 76827700, 2012.
- [47] M. Ruderman and T. Bertram, "Control of magnetic shape memory actuators using observer-based inverse hysteresis approach," *IEEE Trans. Contr. Syst. T.*, vol. 22, no. 3, pp. 1181–1189, 2014.
- [48] M. Shahinpoor and K. J. Kim, "Ionic polymer-metal composites: I. Fundamentals," *Smart Mater. Struct.*, vol. 10, no. 4, pp. 819–833, 2001.
- [49] Q. He, L. Song, M. Yu, and Z. Dai, "Fabrication, characteristics and electrical model of an ionic polymer metal-carbon nanotube composite," *Smart Mater. Struct.*, vol. 24, no. 7, p. 075001, 2015.